

Model Performance Calculation

Ian Keynes

The basic objective of rubber flying is to achieve the maximum duration from a given rubber motor. The alternatives range from slow climbing still air type flying for maximum duration to the greatest climb height possible with a much shorter motor run. Which ever is chosen the principle remains the same - we want to optimise performance from the rubber.

Analysis provides a good way of assessing the multitude of approaches that are possible, and this paper will describe the methods and assumptions I have made in setting up an approximation to the rubber model climb. I concentrate on the method rather than results - just enough of these are shown to give a flavour of what can be studied. Peter King's flow of papers has made several studies of the different questions that can be posed and answered by analysis, including his use of my methods. All modelling works under the big assumption that we can obtain adequate data to set up the mathematical model. Peter's analyses have helped to move the data towards an empirical description of what is observed.

Motor

The starting point is easy to quantify - this is the torque of the given rubber motor as a function of the turns. This must be the torque when unwinding, taking account of the hysteresis compared to the greater torque that is applied when winding the motor (even though the latter is the easier to measure). A typical torque curve is shown in table 1, for a 35g motor of 28 strands. I use units of Newton metres for torque, for those who prefer Imperial units and want to check conversion I have given another column showing the same data in units of in.oz.

turns	Nm	in oz	turns	Nm	in oz
420	0.814	115.3	200	0.110	15.6
395	0.370	52.4	130	0.102	14.4
350	0.211	29.8	70	0.091	12.8
300	0.150	21.2	30	0.070	9.9
250	0.130	18.4	Energy = 423.2		59909

Table 1. Turn-torque data for sample motor.

The torque will be denoted by $Q(n)$ where n is the number of turns remaining on the motor. The torque will have been measured for a motor with a specific mass M_m and a particular number of strands N . It will be useful to explain the possible variations on this basic data according to possible motor changes:

- a) If the motor mass is changed for the same number of strands then the number of turns will change proportionally. For the same torque, i.e. the function $Q(n_1)$ for motor 1 will remain the same as $Q(n_2)$ but will apply for $n_2 = (n_1 M_{m1}/M_{m2})$ turns.
- b) If the number of strands in the motor is changed from N_1 to N_2 , keeping the motor mass the same, then the torque will change proportional to $(N_2/N_1)^{1.5}$ while the number of turns will change according to the inverse of this quantity, summarised as:

$$Q_2 = Q_1 (N_2/N_1)^{1.5} \quad \text{and} \quad n_2 = n_1 (N_1/N_2)^{1.5}$$

Propeller

The motor drives the propeller and, since the basic modelling of the propeller is a subject in its own right, this is described in Appendix A. Repeating the main relationships here, the propeller is defined by the radius, the blade shape (chord and blade angle along the blade) and the aerodynamic characteristics of the blade aerofoil sections. It is assumed here that the thrust T and torque Q can be calculated as functions of propeller advance ratio $\lambda \{=V/(R\Omega)\}$, for forward speed

V , blade radius R and rotational speed Ω . This is most easily implemented via non-dimensional thrust and torque coefficients T_c and Q_c that are calculated as functions of λ and then converted to the dimensional values by the relations (equivalent to Appendix equations A2 and A3):

$$T = T_c \pi \rho \Omega^2 R^4 \quad (1)$$

$$Q = Q_c \pi \rho \Omega^2 R^5 \quad (2)$$

This approximation of T_c and Q_c as functions only of advance ratio neglects Reynolds number effects when the forward speed changes. Depending on how the calculation is implemented it may also neglect variation of section characteristics between the blade tip and sections nearer the root - this simplification is made in the Excel macro version of my calculations. Typical T_c and Q_c curves are shown in figures A3 and A4 in the Appendix.

For any given motor torque $Q(n)$ during the run and any required flying speed V it is possible to find the advance ratio at which the propeller would require this torque to drive it by replacing Ω in equation (2) by λ and interpolating to find the λ for which the following equation is satisfied:

$$\frac{Q_c(\lambda)}{\lambda^2} = \frac{Q(n)}{\pi \rho V^2 R^3} \quad (3)$$

Since $Q_c(\lambda)$ is generally a monotonic decreasing function of λ and we are not concerned with solutions with zero advance ratio, it is generally straightforward to solve this equation by numerical iteration to find the λ which gives the required thrust, and hence from the definition of λ we find the prop rotational speed Ω .

Model dynamics

So far we have defined the motor torque and the propeller that it drives. How the model handles the power depends on the aircraft dynamics, and that is the hardest part to simulate. In reality the aircraft flies in three-dimensional space - if watching from the ground it may move north-south, east-west, and vertically up-down. Viewed from the model the three freedoms are fore and aft, sideways, up and down. There are also three rotational freedoms, usually referenced on the model as roll, pitch and yaw. See figure 1. For movement in any one of these six freedoms the model produces aerodynamic forces and moments with components in all of the freedoms. Many of these are small forces that are difficult to describe precisely in our low Reynolds number conditions, but they can have a powerful effect on the motion. For example, when approaching stall a small

difference between the incidence on right and left outer wing panels may have little effect on overall lift but a powerful effect on yawing moment due to increased drag on one side. A further difficulty is that we operate our models near the limit, so that it is not possible to follow the full-size practice of simplifying the dynamics with linear approximations (e.g. when near the stall the increase in lift due to a positive increment of incidence is not as large as the decrease in lift produced by an equal reduction in incidence).

There are thus massive problems in setting up the detailed aerodynamic model of a model on a varying flight path, with complex aerodynamic interactions between the components of the aircraft compounded by the badly-defined aerodynamics in low speed flight. We must look for some gross simplifications and the first casualty is that we will not then be able to make detailed three-dimensional predictions of the model flight path. A standard simplification made in full-size dynamics is to separate the motions into longitudinal (up-down and fore-aft movement plus pitch rotation) from the lateral (sideways movement and roll and yaw rotations). This approximation assumes that the aircraft is symmetric about the centre-line, often not the case for full-size aircraft but that tends to get disregarded. For a model the asymmetry is normally more fundamental, such as differences of incidence between right and left wings and having a deflected rudder. When the motor is running there are asymmetric effects on the model from the angled and rotating prop-wash. Until we have set up a full prediction of all the aerodynamic forces on the model there is nothing to do but accept the inaccuracies and separate the longitudinal and lateral motion.

For a performance assessment, separating the longitudinal and lateral motion in effect means neglecting the laterals entirely and concentrating on the longitudinal motion. This is because the fundamentals of performance concern the analysis of the climbing (or gliding) model with lift and thrust opposing weight and drag. We know that there are powerful trim interactions that we will miss, e.g. the nose dropping when turning tighter, and we will not be able to make detailed predictions of trim settings. Since longitudinal trim will not be accurate we may make the next step into inaccuracy by neglecting the pitching motion. This leaves us with the up-down and fore-aft freedoms only, corresponding to the key forces being lift, drag and model weight. By neglecting pitching and all lateral motion we effectively assume that by some means or other it will be possible to trim the model to achieve the lift, drag, speed and climb attitude which

we desire. Obviously this will not be possible in all cases, but the aim of the analysis will be to demonstrate maximum performance which could be achieved.

The basic forces acting on the model under this approximation is shown in figure 2 with, for simplicity, the forces shown passing through the CG because pitching has been neglected. For this simplification of the dynamics it does not make much difference which axis system is used but I have followed the form of equations I have chosen for the full motion. This refers the motion to "wind axes", that is the forward direction is in the same direction as the current velocity vector, rather than "body axes" which are fixed in the aircraft. Both axes have their origin at the centre of gravity of the model and the body axis direction is chosen according to convenient features of the aircraft geometry.

The key elements are:

- The velocity is at an angle α to the body axis.
- The thrust T is along a thrustline at angle α_T to the body axis (positive for up-thrust).
- The model mass is m so that weight is mg .
- Aerodynamic forces in the wind axes have components of drag D and lift L .
- The velocity direction is at a climb angle of γ to the horizontal and the body is at angle θ to the horizontal, so that $\theta = \gamma + \alpha$.

The equations of motion can now be written as:

$$m \dot{V} = T - D - mg \sin \gamma \quad (4)$$

$$m \dot{V} \alpha = -(\alpha + \alpha_T) T - L + mg \cos \gamma + m V q \quad (5)$$

These equations define the acceleration along the velocity direction and the rate of change of incidence (which relates to the acceleration component perpendicular to the wind axis plus the effect due to pitch rate rotation). This form assumes that α and α_T are small angles but makes no assumption on the climb angle γ - we need everything up to vertical climb. Pitch rate, q , is the rate of change of the body angle θ so that it is related to the rates of change of the incidence and climb angle by:

$$\dot{q} = \dot{\gamma} + \dot{\alpha} \quad (6)$$

The complete equations governing the model climb are thus (4), (5), (6) plus the use of known torque

value $Q(n)$ in (3) to define advance ratio λ , the thrust coefficient defined in terms of advance ratio (1), and the basic prop speed relationships

$$\lambda = V/(R\Omega) \quad (7)$$

$$\dot{n} = \Omega/(2\pi) \quad (8)$$

The lift and drag of the model must be defined for equations (4) and (5). Represent them via lift and drag coefficients C_L and C_D which must be predicted (guessed) as functions of α and V - one of the unknown areas of the predictions, but which may be tuned to get reasonable climb behaviour and with glide values that are better defined following studies by Peter King and others. Lift and drag coefficients are assumed to have the non-dimensional form:

$$L = .5\rho SV^2 C_L \quad (9)$$

$$D = .5\rho SV^2 C_D \quad (10)$$

where ρ is air density and S is a reference area (usually wing area).

A sample polar is shown in figure 3 from data given in table 2. With poor information about our models it is not realistic to specify lots of points around the polar, but it is necessary to include reasonable detail or accurate values around the glide condition. Maximum glide duration is obtained for the incidence which gives a minimum value for the function $C_D^4/(C_L^2 + C_D^2)^3$. For the sample data the optimum glide is with $C_L=1.0$ and this corresponds to $C_D=0.063$. If the

model has area 0.16 m^2 , mass 0.23 kg and air density is 1.22 kg/m^3 then glide speed is 4.8 m/sec and V_G , the vertical rate of descent in the glide, is 0.3 m/sec .

CD	CL	CD	CL
0.069	-0.1	0.053	0.8
0.059	0.0	0.057	0.9
0.050	0.2	0.063	1.0
0.046	0.4	0.077	1.1
0.048	0.6	0.108	1.2

Table 2. Sample CL-CD polar for model.

form of (4) and (5) is complicated by the appearance of the pitch rate, since we have already decided that we do not have enough information on the aerodynamic moments which govern the pitch rate. There are a number of useful simplified forms that will now be described.

Solution of the equations of motion in the

Vertical Climb

One simplification is for vertical climb, for which the thrust is directed upwards to balance the weight downwards. If the model has up-thrust or downthrust then there will need to be a small lift force (down or up relative to the model) to offset the normal component ($T\alpha_T$) of the thrust, but since we assume the thrustline angle α_T is small then it follows that the drag in this condition is unlikely to be very different from the true zero lift drag. The vertical motion is described by the reduced form of (4) as:

$$\dot{m}V = T - D_0 - mg \quad (11)$$

The drag D_0 is the zero lift drag and this is obtained directly from your value for the zero lift drag coefficient of the model C_{D0} (taken to be independent of Reynolds number so that it is a constant that does not vary with V):

$$D_0 = .5\rho SV^2 C_{D0} \quad (12)$$

Assume that the launch velocity is known, so this provides the initial condition for the solution. If the model has a delayed prop release the initial velocity decay is easily calculated by solving equation (11) with thrust $T=0$ and the airspeed dropping as a result of the combined action of the model weight and drag. At some time the prop must start and the thrust T is then a function of airspeed V and propeller rotational speed Ω . The airspeed at this time will have been calculated as just described (or if there was no prop delay the airspeed will be the launch speed). Assume that the prop instantly accelerates up to a rotation speed appropriate to this current airspeed V and the applied torque $Q(n)$. Solve equation (3) to find the advance ratio λ that applies for these conditions - then calculate the thrust coefficient T_c for this advance ratio and hence find the thrust T from equation (1), noting that the propeller rotational speed Ω is given by equation (7).

The equation of motion can now be solved by conventional differential equation methods to produce the time history as the model accelerates and decelerates in the vertical climb. In words, the acceleration is found by evaluating the forces on the right hand side of equation (11) and dividing by the mass. At the end of some time interval δt (a small fraction of a second) the acceleration will have increased the airspeed to a new value $V+\delta V$, the prop will have rotated through an angle of $\Omega \delta t$ radians, so that from equation (8) the number of turns on the motor will have decreased by $\delta n = \Omega \delta t / (2\pi)$ revs and the new motor torque will be

$Q(n-\delta n)$. Equation (11) is now solved again to find the new acceleration value given the initial velocity $V+\delta V$ and the torque $Q(n-\delta n)$.

The solution is then repeated as long as required; subject to the model still having turns on the motor and adequate thrust to maintain an upward vertical airspeed. We will discuss transition from the vertical climb later, but first review some sample vertical climb results.

The results are for a standard F1B with DPR set so that the prop starts 0.2 sec after launch. An Andriukov prop with 0.3m radius has been used with a 28-strand motor. CL-CD values used for the model and the propeller are based on previous estimates by Peter King and myself. Figures 4 and 5 show the vertical velocity and height for three different launch velocities 4, 8 and 12 m/sec.

The first point on the plots is at 0.2 sec, the time at which the prop starts. The velocity has dropped to 2 m/sec from the 4 m/sec launch, while the highest speed launch has slowed from an initial 12 to 9.25 m/sec. Most of the reduction is due to gravity and a smaller part due to model drag - as shown by the larger speed drop for the higher launch speed (more drag at higher speed). After the prop has started all three cases show a similar acceleration, gradually tailing off to give a peak speed about one second after launch. Not surprisingly, the lowest launch speed reaches a lower peak speed and the detectable velocity difference lasts until just after two seconds. The height difference between the highest and lowest speed launches is about 7m. Note that these plots have been continued to the bitter end when the speed has dropped to almost nothing - a real model would have had to drop its attitude below vertical by about the 4-second stage.

Look now at the effect of changing prop pitch for one launch speed, chosen to be 8 m/sec. As the simplest way to achieve this in the simulation is by rotating the prop blade (variable pitch style) the blade angle has been changed by +5 and -5 degrees from nominal - really showing the effect of VP adjustment rather than a true geometric change of prop pitch. First, figure 6 shows the effect of these prop changes on the thrust developed at different airspeeds. This plot is for an applied torque of 0.435 Nm, which is the torque applied by the motor in this example just over one second after the prop started. As you would expect, the low pitch prop develops most thrust at low speed - almost double the high pitch prop, which is operating with most of its blade at high angles of attack and effectively stalled. As speed increases from zero the

thrust of each prop increases; the low pitch prop peaks first at 5 m/sec while the high pitch one continues to increase thrust up to 9 m/sec. Thereafter the decline from the peak is lowest for the high-pitch prop, which becomes the prop with most thrust for speeds above 16 m/sec (which is above the speed range of interest in this example).

This insight into the prop thrust characteristics explains the differences seen in vertical climb performance in figures 7 and 8. The increased pitch prop +5 degrees reaches a lower peak speed at 1 sec. and finishes up at a lower altitude. This results directly from its lower thrust at low speed and consequent slower acceleration from the residual speed of 5.7 m/sec when the prop starts. It would appear to be a clear-cut choice that the high pitch prop is not best for this part of the climb. However, it is not so clear-cut because it has been turning more slowly and thus consuming less energy than the other props. To demonstrate this figure 9 shows the same results plotted against turns remaining on the motor instead of time.

This shows that the high pitch prop and the nominal prop achieve very similar height at the same turns. In fact the high pitch prop is slightly better (1.5m higher) than the nominal prop at the 375 turns stage. The high pitch prop model reaches this stage 3 seconds after launch, which is a realistic finish time for vertical climb.

The low pitch prop has been consistently at the lowest height of the three props at the same number of turns. It eventually reaches the highest height at the end of its curve, but this has been at the cost of using more turns, which would leave less energy for the later climb.

These calculations were made on a nominal Andriukov prop with pitch changed by rotating the blade +5° and -5°. To examine the inefficiency of changing pitch in this way compared to studying a new prop with a different pitch, the same calculations were run for props with similar helical pitch distributions along the blade. By setting the pitch from the original prop angle at 80% radius, the helical props had pitch/diameter ratios of 1.22 nominal prop and 1.5 for the high pitch and 1 for the low pitch prop. There was typically less than 1% difference in the height between the helical props and the ones described earlier and all of the relative trends between the props were preserved closely.

The vertical climb solution process can continue until all the turns have run down (very unlikely) or until the airspeed has dropped to zero. Obviously at some point the model should pitch down so that the air-

speed can be maintained before this happens. We can take two approaches here:

- Assume that the VIT time is known and the model leaves the vertical climb at that time. In fact the change of VIT will produce a nose-up moment which, in our simple approximation would take the model beyond vertical, but in reality the combination of pitch and roll will turn the model into a steep climb (one of the reasons we dropped any attempt to simulate the pitching motion directly).
- Calculate the optimum time to leave vertical flight. I have adopted this option in my optimum performance calculations. The process, described below, looks at the relative efficiency of each segment of the vertical climb compared to the equivalent non-vertical climb in terms of adding height or duration for the amount of rubber energy used. The vertical climb ends when it ceases to be the most efficient flight path.

Steady climb

Whichever approach is used to determine when vertical climb ends, it will be necessary to build a simulation of the non-vertical climb. We will now look at this solution of the equations for climb below the vertical.

A simple approximation is to assume that at any time the model is in a steady climb. This means that the derivatives on the left of (4) and (5) and also the pitch rate q are all neglected and the equations reduce to the algebraic form:

$$T - D = mg \sin \gamma \quad (13)$$

$$(\alpha + \alpha_T)T + L = mg \cos \gamma \quad (14)$$

These equations require that all the flight parameters remain constant during this period of steady climb, that is, the drag, lift, climb-angle and airspeed. The solution of these algebraic equations is different from the differential equations for the vertical climb; it is not a true progression with time but a snapshot approximation at a specific time. My approach has been to assume the climb may be subdivided into a number of separate snapshots, each one corresponding to a flight segment of maybe 20 turns run down on an F1B motor. The average torque in this segment is known and the equations solved for that average torque value, as if the torque curve was a series of step values (figure 10).

The $(\alpha + \alpha_T)T$ term in equation (14) is slightly awkward since it needs an estimate of the incidence α

at which a particular lift is generated, which is an extension over the already significant problem of estimating the CL-CD polar itself. The approach taken in my current release of Excel macros is to neglect the term: when the climb is steep then there will be no problem generating enough lift with or without the increment due to the thrust component. At a lower climb angle then the thrust is smaller - significantly less than either the lift or the weight - and, combined with the factor $(\alpha + \alpha_T)$ reducing the term further, the term does not make a large difference to predictions. Typically it can correspond to a 5% change in the CL required at the end of the climb and that is within the range of uncertainty for CL.

I have developed an extension to include the effect in the solution of equation (14) by assuming that a constant lift curve slope $C_{L\alpha}$ describes the lift coefficient between zero lift incidence α_0 and an α corresponding to CL_{max} so that an estimate of α may be calculated from:

$$L = .5\rho SV^2 (\alpha - \alpha_0)C_{L\alpha} \quad (15)$$

so that:

$$\alpha = \alpha_0 + L / (.5\rho SV^2 C_{L\alpha}) \quad (16)$$

There are generally many solutions of equations (13) and (14), i.e. everything between flying at slow airspeed in a steep climb to flying fast in a steep dive. This is demonstrated in the following example for an F1B in an early cruise condition with torque 0.29 Nm. On my example model and motor this corresponds to the interesting period around 4 or 5 seconds after launch when there is the option of continuing in a vertical climb or at a lesser angle.

From equations (1), (2) and (3) the thrust and airspeed are found which correspond to a range of advance ratio λ for this required torque. This gives a range of thrust and velocity values that satisfy the prop equations for this torque, shown in figure 11.

For each of these velocity values we can assume a drag coefficient in order to find the drag from equation (10) and then equation (13) can be solved to find the climb angle. This climb angle can be substituted into equation (14) to find the required lift and, since the velocity is known, this gives the required lift coefficient CL . From this CL the drag coefficient value can be refined and the iteration repeated until a consistent result is found. The prop speed can be found from the definition of the advance ratio. The resulting climb angle as a function of speed is shown in figure 12.

Because of the v-squared increase in drag the solution for 15 m/sec is actually a dive - not very interesting for best performance! As the speed is reduced the climb angle increases until it reaches the 90° vertical for a speed of 6.24 m/sec. For speeds just lower than this there is no steady climb solution - because the model would actually accelerate. As we study lower and lower speeds eventually we come to another vertical solution at 3.08 m/sec. Below that there is a narrow window with steady climb solutions at steep angles, and that finishes at 2.4 m/sec. The drag is small at these low airspeeds so the major force balance is between thrust and weight; as the climb angle drops below vertical then lift is also needed to hold the model up, reaching the CLmax limit by 2.4 m/sec.

A measure of the efficiency of the climb is given in figure 13 which shows the height gained per turn unwound from the motor. At the highest speed shown the height gain is negative (as seen already via the nose-down "climb" angle) and, as the speed drops, peak efficiency is reached at 7.1 m/sec with a climb angle of 67°. Slower speeds (steeper climb angles) are slightly less efficient and the curve stops at 6.24 m/sec when the 90° climb is reached. The short region of low speed steep climb is seen to be half as efficient - not surprising, since we are familiar with slow, hanging-on-the-prop situations that have a greater element of impending disaster than efficient climb!

Optimum Climb Segments

Return now to selecting the solution of equations (13) and (14) from the range of possibilities. If a desired climb angle is specified then the airspeed can be found at which this climb could be flown (if is not too steep for the available power). My regular analysis takes the alternative approach of examining all possible climb angles and selecting the most efficient climb angle for the segment. Let Δn denote the number of motor turns in the segment and Δt the time spent in running off these Δn turns. From the speed V and the climb angle γ the vertical speed component is $V \sin \gamma$ and so the height gained in the segment is $\Delta t V \sin \gamma$. Efficiency of the climb is defined as either the maximum height gain in the segment or the maximum duration added (the time taken to run off the turns in this segment plus the time to glide down from the height gained). These can be measured by the "per motor turn" efficiency factors:

$$[(\Delta t V \sin \gamma)/\Delta n] \text{ for height}$$

or:

$$[\Delta t (1 + (V \sin \gamma)/V_G)/\Delta n] \text{ for duration.}$$

These factors are used for comparisons within a segment when a given amount of torque (and energy) is available from the motor. We have already seen the height efficiency demonstrated for one segment in figure 13. When comparing between segments to find which segment is the most effective, account must be taken of the energy available by considering instead the height gain per unit energy or duration gain per unit energy, rather than "per turn" quantities.

The Excel macro implementation of the complete process consists of the following steps:

- 1) Read in data on prop, motor and model.
- 2) Process the CL-CD polar to find the optimum glide conditions and hence the glide descent rate V_G .
- 3) Evaluate the propeller thrust and torque coefficients T_c and Q_c for a full range of advance ratio, ranging from a very small value up to a value at which the thrust has become negative.
- 4) If there is a delayed prop release process the vertical motion of the model up to the time the prop starts.

For each torque segment of the motor data do steps 5 and 6:

- 5) For each of the prop advance ratio values:
 - a) Solve equation (3) to find the airspeed V that corresponds to this advance ratio and the torque of the current segment, hence find the thrust T for each advance ratio.
 - b) Search round the CL-CD polar to find a combination of lift and drag coefficients (hence L and D for the known speed V) and climb angle (which allows a solution of equations (13) and (14) - if there is a suitable combination to solve the equations. If thrust is excessive then the only solution may be vertical climb.
 - c) Evaluate the efficiency of the solution for this advance ratio, either based on height gain or duration gain.
- 6) From the array of results from step 5(c) choose the advance ratio which gives the most efficient climb. From the climb angle, model airspeed and prop speed for this advance ratio calculate the time it will take to run off the segment number of turns and the height gain. If the vertical climb is most efficient then make the detailed analysis of vertical climb for this segment. From either source you get the flight time and model height at the end of this segment

- 7) At the end of this process for all the torque segments the final result is the time of the motor run and the height reached at prop fold. From the glide descent rate V^G the descent time from this height can be calculated and hence the total flight time.

Optimum climb example

The results from a sample F1B optimum climb calculation are given in table 3 at the end of the paper. This is for the prop that we have studied earlier with a pitch/diameter ratio of 1.2. The number of torque segments for the 35g motor has been kept small in order to minimise the amount of data to present.

The vertical climb has been calculated precisely following launch at 8 m/sec and a 0.2 sec DPR and has been continued for those torque segments for which the total performance in the vertical climb in the segment is better than the best non-vertical steady climb in that segment. Thereafter the non-vertical steady climb is used for each segment. This is the same model and prop which were used as an example of steady climb and shown in figures 12 and 13 with the torque corresponding to the second segment on this motor. In the latter figure it was seen that a climb at 67° was slightly more efficient than a steady vertical climb with that torque, but table 3 shows that the vertical climb has been selected as the most efficient. This is because the comparison here is with the more detailed vertical climb analysis, which for this segment had started with a speed of 12 m/sec dropping to about 5 m/sec by the end of the segment and, compared to a steady climb approximation giving 7.7 m/sec, this gave a slightly higher climb.

The application of the analysis is demonstrated in figures 14, 15, and 16, which show some of the results for a comparison of three cases that are identical except for having propellers with pitch/diameter ratio 1, 1.2, and 1.4. Results for the three cases were respectively: motor run 39.6, 44.3, and 49.1 sec; total duration 338, 365, 366 sec; maximum height during the run 90.4, 97.1, and 96.0m.

In figure 14 it is seen that the high pitch prop operates at the lowest lift coefficient and it is seen from figure 15 that this model flies fastest. Climb attitude is not shown here but is almost identical for each prop except that the high pitch prop only holds vertical climb for the first segment. Notice that the P/D=1 prop has, for some reason, chosen to finish the climb at a CL slightly greater than the glide CL. These calculations were optimised on height and the measure of that, height gain per unit energy, is plotted in figure 16. Reflecting the lowest total height, the P/D=1 prop is

poorest for most of the time. The P/D=1.4 prop is slightly poorer than the 1.2 prop at the start (when it cannot hold a vertical climb) and appears to be better later, but that is really an illusion resulting from the longer run of the high pitch prop; if plotted against turns instead of torque the later climb efficiencies are almost identical.

Specified climb profile

The optimum process in the last section has defined a climb consisting of optimised steady segments. The assumption has been made that the model can be trimmed to follow the required climb profile and that it can adapt to the required airspeed at each time. However, there is no guarantee that this is completely feasible. Within our assumption that pitching motion is neglected we cannot answer the question about trim, but we can address the motion of the model as affected by the values at every instant of torque, airspeed, prop thrust and climb angle. Mathematically this is done by solving equations (4) and (5) for a specified climb profile. This climb profile may be the one resulting from the optimum climb calculations or it may be one chosen by the user.

There is a choice of specifying either the flight path angle γ or the body axis angle θ , related through $\theta = \gamma + \alpha$. The choice made here is the flight path angle, since this is more directly related to the motion (vertical is straight up) without assumptions of zero lift angle. Another choice to be made is the terms in which the required flight path angle is specified - the obvious variables being either time or motor turns.

The solution technique is similar to that used for the vertical climb - continually solve the differential equations as the motor turns reduce in small stages. Indeed, for a vertical launch the process is identical up to the time that the specified climb angle drops below the vertical. The method then extends to covering both equations (4) and (5) for the climb at other angles.

From the current airspeed V and the applied torque $Q(n)$ solve equation (3) to find the advance ratio λ which applies for these conditions. Then calculate the thrust coefficient T_c for this advance ratio and hence find the thrust T from equation (1), noting that the propeller rotational speed Ω is given by equation (7). The only unknown remaining in equation (4) is now the drag. This will be defined by calculating the lift required and hence the related drag from the CL-CD polar. Equation (5) involves the pitch rate and the rate of change of the incidence; the difference between these two terms is equivalent to the rate of change of flight path angle from $\theta = \gamma + \alpha$ remembering that

pitch rate q is the rate of change of θ . Re-writing equation (5) in this form and re-arranging in terms of the unknown L and repeating equation (4) gives the pair of equations to be solved as:

$$m\dot{V} = T - D - mg \sin \gamma \quad (4)$$

$$L = -mV\dot{\gamma} - (\alpha + \alpha_T)T + mg \cos \gamma \quad (17)$$

At any stage the flight path angle γ is known (interpolation between the specified values to the time or turns at that stage) and it should be a smooth function in order to give a continuous value for the rate of change term. The thrust T is known from the torque and airspeed as described in the last paragraph. The remaining problem is the $(\alpha + \alpha_T)$ factor on the thrust. As discussed in the steady climb section this is a relatively small term and may be approximated via equations (15) and (16).

In practice I have found that the process may be sensitive - effectively you trim the climb by tweaking the climb angle at different times. Indeed, starting from the values of climb angle from the optimised climb it took quite a few trials before reaching a reasonable climb. One of the problems is that if the climb is required to be too shallow the speed builds up and so the lift coefficient can drop. On the other hand, if the climb is slightly too steep the solution the limits of maximum lift coefficient and low speed. This latter case showed up the inaccuracy of neglecting pitch: if the speed has dropped so much that the necessary lift coefficient cannot be reached then the equations rightly tell the model to drop below the climb angle and pick up speed. However, without any pitch term this is done instantaneously - the nose drops to a 20 degree dive, speed picks up a fraction of a metre per second and perhaps a twentieth of a second later the lift coefficient comes within reach and the climb resumes. Without pitch inertia this is on an unrealistically short time-scale and small loss of height, but otherwise just what would happen.

Sample results are given in table 4 for the same P/D=1.2 climb shown in the

optimised steady climb table 3. Note that the mean values in the left-hand columns are time-averaged rather than the optimum climb segments which are turn-averaged. This leads to differences in relative sum magnitudes. The detail differences are interesting but the bottom line is that the height is very little less than the steady climb optimum - providing some confirmation of the value of that analysis.

Conclusion

I have described my approach to calculating rubber model performance. Such analyses are not precise, make significant simplifications and are still limited by the quality of the data available. Even so, I think that such studies can help our understanding of the relative importance of the many factors.

The analyses described here are available as Excel macros, contact the author for further details at kaynes@compuserve.com.

List of Symbols

C_D	drag coefficient, defined in equation (10)
C_{D0}	drag coefficient at zero lift
C_L	lift coefficient, defined in equation (9)
C_{Lmax}	maximum lift coefficient
$C_{L\alpha}$	slope of lift curve per radian
D	drag, aerodynamic force in opposite direction to velocity, N
D_0	drag at zero lift, N
g	gravitational constant
L	lift, aerodynamic force perpendicular to velocity, N
m	model mass, Kg
M_m	mass of rubber motor, Kg
n	number of turns
N	number of strands in rubber motor
Q	torque of rubber motor, Nm
Q_c	propeller torque coefficient, see equation (2)
R	propeller radius, m
S	reference area, m^2
T	propeller thrust, N
T_c	propeller thrust coefficient, see equation (1)
V	airspeed, m/sec
α	incidence, the angle between aircraft velocity and the body axis, radian
α_0	incidence for zero lift
α_T	up-thrust, angle of thrustline to the body axis, radian
γ	climb angle, angle of the velocity direction to the horizontal, radian
θ	Climb attitude, angle of body axis to the horizontal
λ	propeller advance ratio $= V/(R\Omega)$
ρ	air density, Kg/m^3
Ω	propeller rotation rate, radians per sec
\dot{x}	denotes the rate of change of x with time

These columns are mean values in segment						These columns are values at end of segment					
mean torque	advance ratio λ	prop rev./sec.	air speed V m/s	climb angle γ deg.	CL	turns	height m	time sec.	height gain in segment m	height gain per unit energy	duration gain per unit energy
launch			8.00			420					
end DPR			6.89	90.00	0.00	420	1.35	0.20	1.35		
0.592	0.282	20.84	11.08	90.00	0.00	395	14.64	1.40	13.29	0.175	0.593
0.290	0.280	14.56	7.70	90.00	0.00	350	38.43	4.49	23.78	0.250	0.866
0.180	0.269	11.20	5.68	35.04	0.59	300	52.98	8.96	14.55	0.233	0.849
0.140	0.272	9.87	5.06	25.75	0.81	250	64.11	14.02	11.13	0.245	0.927
0.120	0.274	9.15	4.73	21.17	0.96	200	73.45	19.49	9.34	0.243	0.951
0.106	0.287	8.70	4.70	17.18	1.01	130	84.61	27.53	11.17	0.239	0.965
0.096	0.298	8.41	4.73	14.31	1.01	70	92.95	34.66	8.34	0.230	0.958
0.080	0.309	7.81	4.55	10.13	1.10	30	97.06	39.79	4.10	0.199	0.912
0.035	0.384	6.34	4.58	-0.67	1.10	0	96.80	44.52	-0.25	-0.036	0.599
Total flight time=365.0			Glide time=320.5			Energy in motor=423.2 or 312 ft.lb.					

Table 3. Performance predictions for F1B with prop pitch/diameter=1.2 by optimum steady segment analysis.

These columns are mean values in segment						These columns are values at end of segment					
mean torque	advance ratio λ	prop rev./sec.	air speed V m/s	climb angle γ deg.	CL	turns	height m	time sec.	height gain in segment m	height gain per unit energy	duration gain per unit energy
launch			8.00			420					
end DPR			6.87	90.00	0.00	420	1.35	0.20	1.35		
0.582	0.283	21.19	11.25	90.00	0.00	395	14.68	1.38	13.33	0.203	0.685
0.285	0.284	14.47	7.82	80.80	0.47	350	38.37	4.50	23.69	0.227	0.792
0.179	0.271	11.21	5.72	34.75	0.69	300	52.84	8.96	14.46	0.255	0.925
0.140	0.281	9.91	5.24	25.18	0.83	250	64.07	14.00	11.27	0.252	0.948
0.120	0.279	9.16	4.82	21.35	1.05	200	73.65	19.46	9.58	0.248	0.965
0.106	0.282	8.64	4.59	17.28	1.01	130	84.68	27.56	11.03	0.238	0.962
0.096	0.296	8.36	4.66	14.19	0.93	70	92.86	34.74	8.18	0.229	0.955
0.080	0.332	8.13	5.08	8.70	0.88	30	96.64	39.66	3.77	0.191	0.877
0.034	0.399	6.49	4.83	-0.41	0.98	1	96.51	44.08	-0.13	-0.042	0.551
Total flight time=363.6			Glide time=319.5			Energy in motor=423.2 or 312 ft.lb.					

Table 4. Performance predictions for F1B with prop pitch/diameter=1.2 by specified climb angle. Note that this analysis is time accurate not segment averaged, results are shown here at end of the same turn segments as table 3 for comparison.

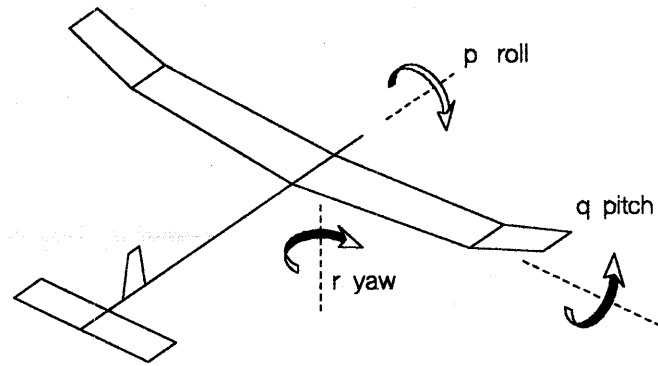


Figure 1. Aircraft rotations in 6 degrees of freedom motion.

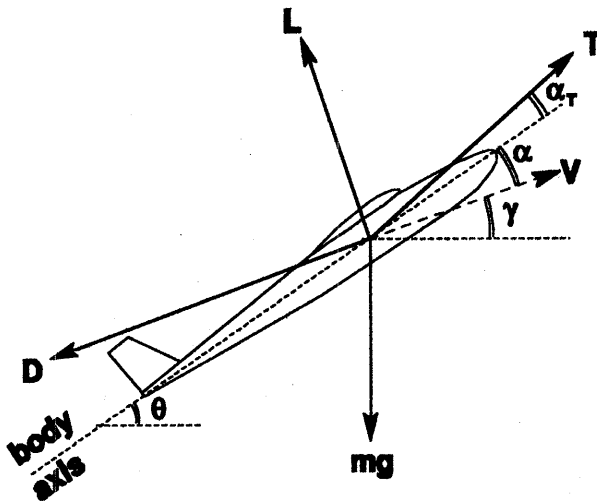


Figure 2. Balance of forces in climb.

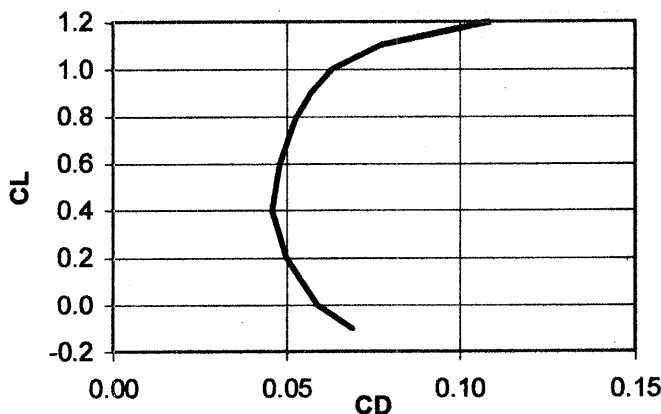


Figure 3. Sample CL-CD polar.

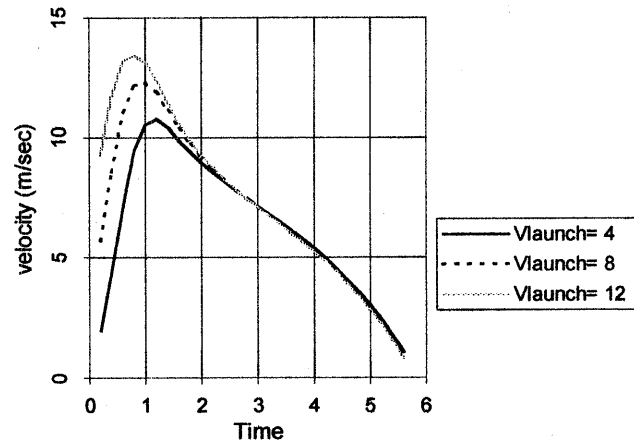


Figure 4. Velocity in vertical climb from different launch speeds.

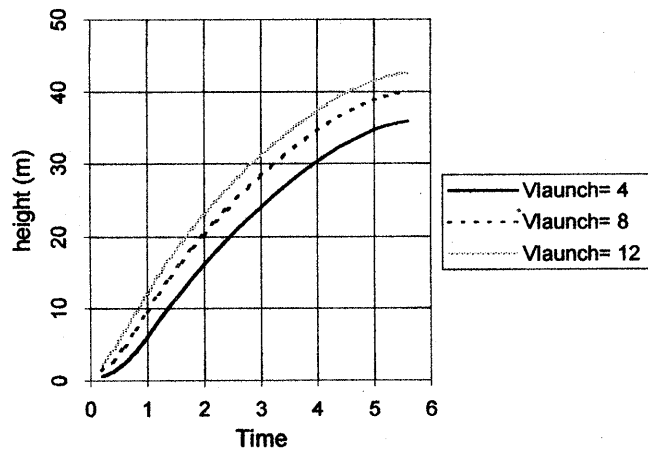


Figure 5. Height in vertical climb from different launch speeds.

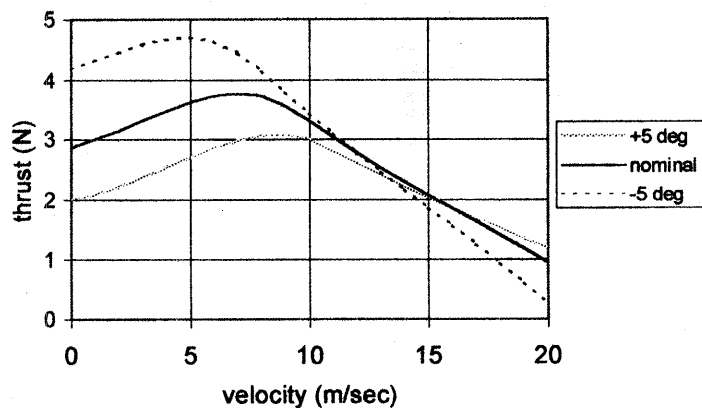


Figure 6. Effect of prop pitch on thrust with airspeed for torque 0.435 Nm.

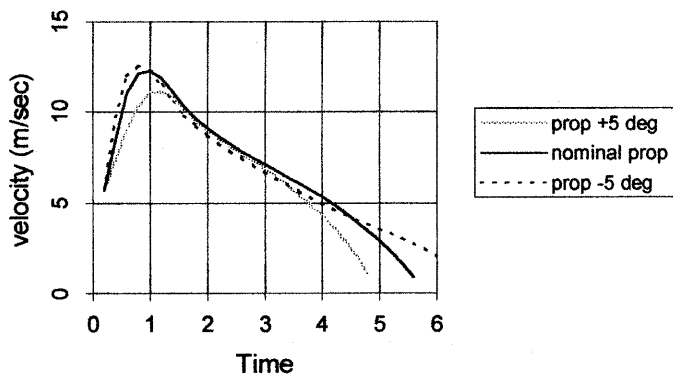


Figure 7. Variation of velocity with time for different prop pitch,
 $V_{\text{launch}}=8 \text{ m/sec}$.

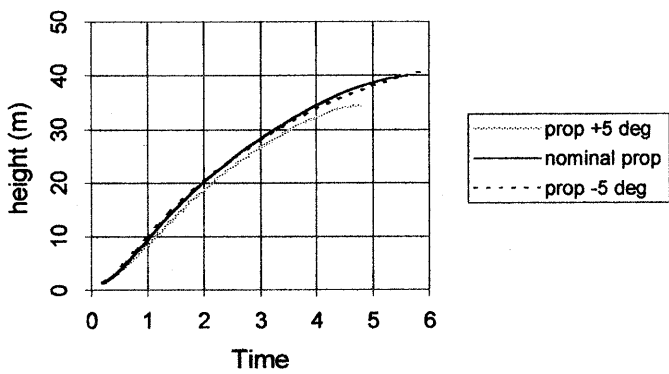


Figure 8. Variation of height with time for different prop pitch,
 $V_{\text{launch}}=8 \text{ m/sec}$.

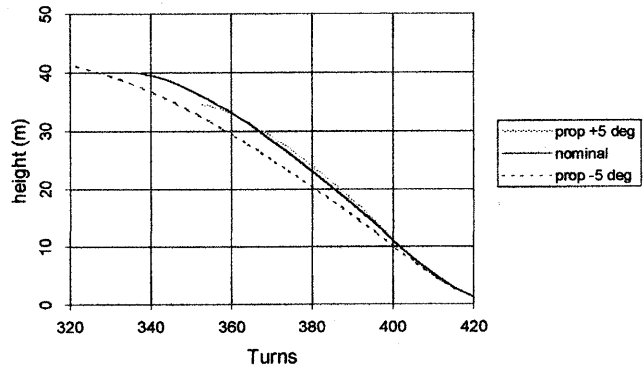


Figure 9. Variation of height with turns for different prop pitch,
 $V_{\text{launch}}=8 \text{ m/sec}$.

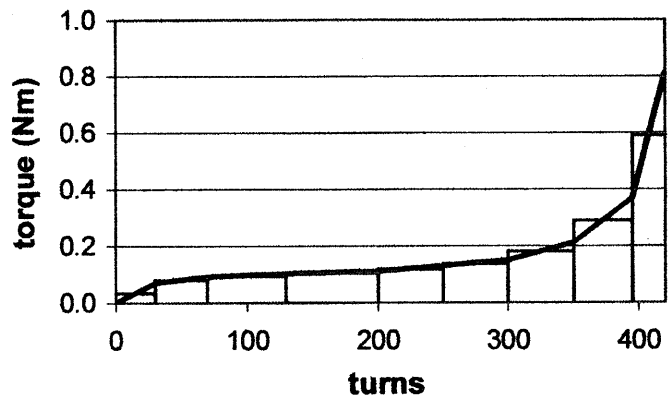


Figure 10. Approximation to torque curve for segment optimum performance method.

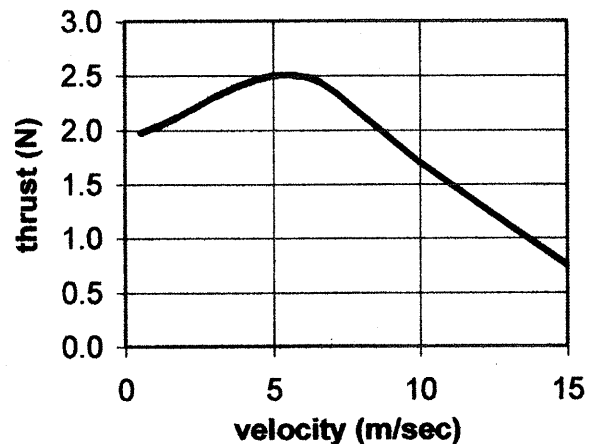


Figure 11. Variation of thrust with flight speed for torque 0.29 Nm.

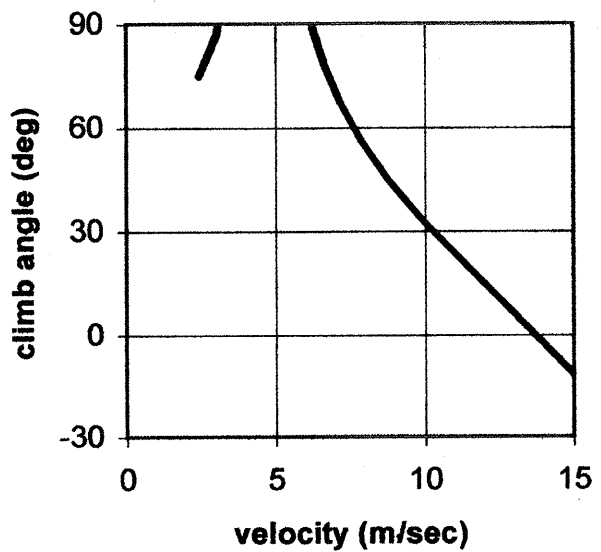


Figure 12. Variation of steady climb angle with flight speed,
torque 0.29 Nm.

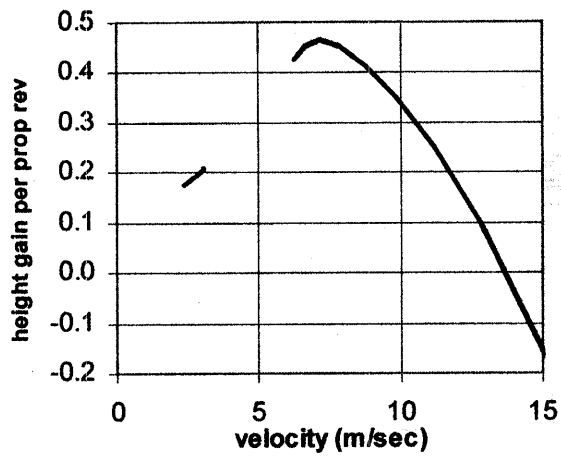


Figure 13. Variation of climb efficiency with flight speed for $Q=0.29 \text{ Nm}$.

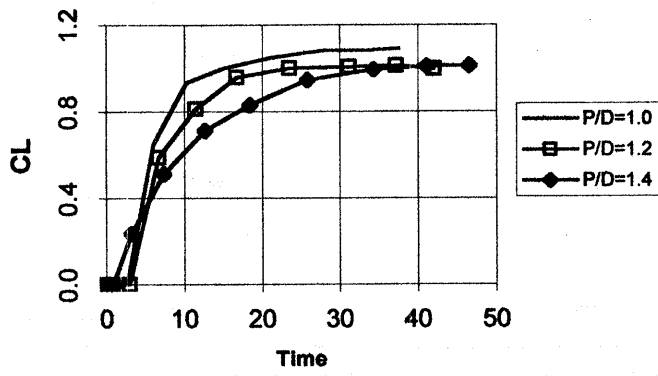


Figure 14. Model lift coefficient for 3 props (optimum steady segments).

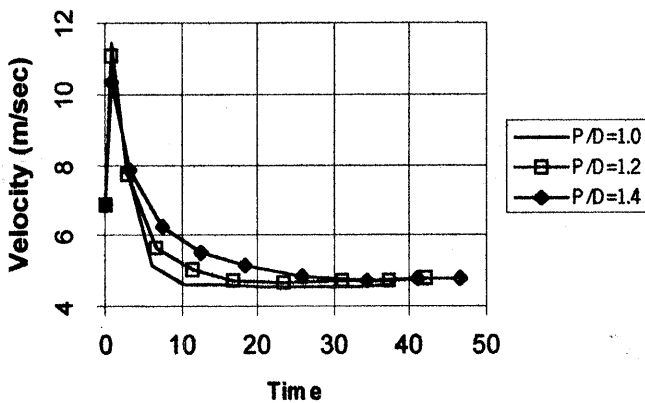


Figure 15. Model velocity for 3 props (optimum steady segments).

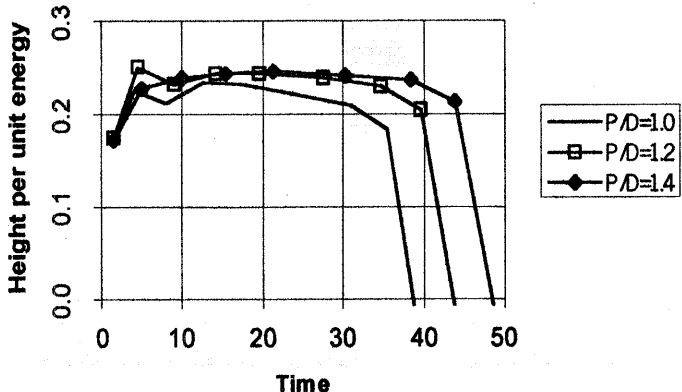


Figure 16. Height gain per unit energy for 3 props (optimum steady segments).

Appendix A: Propeller theory

The standard textbooks on aerodynamics describe propeller theory generally in the classical forms developed during the twenties and thirties when props provided the motive power source of all full-size aircraft. The fundamentals and particularly the approximations sometimes invoked are not necessarily appropriate to model propellers but there are not many alternative approaches which are better! To explain some of the principles of propeller operation, I will give a brief account of the various representations of props starting with the simplest idea of the fundamentals through to more detailed simulations. This follows the approach by Glauert as given in ref.1.

Introduction

A propeller consists of a number of equally spaced identical radial blades that are maintained in uniform rotation about the axis of the propeller by the torque of the engine.

The aerofoil section of each element of a blade produces lift and drag forces that combine to form the thrust and torque of the propeller. The reaction of these forces on the air produces a slipstream comprising all the air that has passed through the circle swept by the rotating blades. The propeller torque corresponds to rotational velocity imparted to the air and the thrust is obtained by imparting a backward linear momentum to the air in the slipstream. The thrust is the direct result of the propeller creating an increased air pressure immediately behind the disc and a lower pressure in front. The axial velocity through the propeller increases from some way in front to reach a maximum some distance behind the prop, and correspondingly the slipstream contracts as shown in figure A1.

This is the view as seen moving with the prop through the air at speed V , or alternatively watching a stationary prop in a wind tunnel with air being blown past at an initial speed V .

The engine applies the torque Q and it turns the prop at angular velocity Ω ; thus the prop absorbs power ΩQ ; The thrust T acts to move the aircraft forward at a speed V , which is measured as useful work VT . The efficiency η is the ratio of power absorbed to useful work, that is:

$$\eta = \frac{VT}{\Omega Q} \quad (\text{A1})$$

In the analysis of propellers it is convenient to remove the dimensions of the quantities by defining the following coefficients:

Speed ratio λ which relates the forward speed to the rotational speed $\lambda = V/(\Omega R)$ (this is the ratio of the forward speed to the rotational speed at the tip and thus equals the tangent of the tip advance angle. Note: alternative terminology uses the parameter $J = V/nD$, so that $J = \pi \lambda$).

$$\text{Thrust coefficient } T_C = \frac{T}{\pi \rho \Omega^2 R^4} \quad (\text{A2})$$

$$\text{Torque coefficient } Q_C = \frac{Q}{\pi \rho \Omega^2 R^5} \quad (\text{A3})$$

where R is the radius of the propeller and ρ the air density. Note that these coefficients lead to an alternative form for the definition of efficiency:

$$\eta = \frac{\lambda T_C}{Q_C} \quad (\text{A4})$$

Axial momentum theory

The propeller develops thrust by imparting a velocity to the air and the thrust is directly related to the kinetic energy of the air motion. Additional energy is dissipated by the production of rotational motion and the frictional drag losses, but for an idealised propeller the axial momentum theory neglects these. Under this Rankine-Froude theory the velocity is assumed uniform over a disc at any part of the wake. The thrust is given by $T = S_1 \rho u_1 (u_1 - V)$ where S_1 is the cross sectional area of the wake well behind the propeller, u_1 is the final velocity in the wake and V is the initial inflow velocity upstream of the propeller. The power is the increase in kinetic energy $P = \frac{1}{2} S_1 \rho u_1 (u_1^2 - V^2)$. Continuity and other considerations lead to the deduction that the velocity u at the prop disc is the mean of the inflow and far wake velocities, that is:

$$u = .5(V + u_1) \quad (\text{A5})$$

The efficiency is then:

$$\eta = V/u \quad (\text{A6})$$

It is seen that the most efficient propeller is one with the value of u only just above V , that is a small increase in air velocity. To generate a given amount of thrust this requires a large diameter - the reason a helicopter has a large diameter rotor for greater efficiency than typical propellers.

An alternative terminology for the velocities is to denote u by $V(1+a)$ where a is the axial interference factor and represents the increase of velocity at the propeller disc. In this form the efficiency equation becomes:

$$\eta = \frac{1}{(1+a)} \quad (\text{A7})$$

Momentum theory development

The first improvement from the axial momentum theory is to remove the assumption that the thrust is uniformly distributed over the entire propeller disc. By considering the momentum equations for each annular ring making up the disc, similar thrust and power equations to those above can be developed for each ring. Then it is possible to define a propeller with ideal efficiency by redistributing thrust between the different rings. The result found is that the uniform disc loading gives the most efficient propeller, with the ideal efficiency the same as given in the last section, i.e.:

$$\eta_1 = \frac{1}{(1+a)}$$

and the corresponding thrust and torque coefficients are:

$$T_C = 2a(1+a)\lambda^2 \quad \text{and} \quad Q_C = 2a(1+a)^2\lambda^3$$

or, expressed in terms of the ideal efficiency η_1 :

$$T_C = \frac{2(1-\eta_1)\lambda^2}{\eta_1^2} \quad \text{and} \quad Q_C = \frac{2(1-\eta_1)\lambda^3}{\eta_1^3}$$

These expressions can be useful in showing the maximum limit to the prop characteristics.

General momentum theory

This theory introduces the rotational motion imparted to the slipstream by the propeller, and this motion corresponds to further energy losses. The actuator disc

concept is extended so that the disc can impart a rotational motion to the air as well as an axial velocity.

Relationships can be developed linking the axial and angular velocities in axial rings of the wake. The problem knows the actual distribution of one or other the two velocities. Assumptions often adopted are based on the fact that the angular velocities are generally small, particularly compared to Ω the angular velocity of the prop. If it is assumed that the flow is irrotational at all points except the axis (that is, angular velocity ω varies with the radius r such that the rotational momentum ωr^2 is constant for all values of r) then the axial velocities u are the same across a complete disc of the slipstream. In this case the axial velocity at the prop is slightly greater than the mean of the inflow and final values given in equation (A5), so that $u > .5(V+u_1)$.

The rotational interference factor a' at a radial location is defined as half the ratio of local angular velocity to prop angular velocity, that is $a' = .5 \omega / \Omega$. The efficiency of an annular element is then given by an extension of (A7) as:

$$\eta = \frac{1-a'}{1+a} \quad (\text{A8})$$

It is possible to derive expressions for ideal efficiency of the annular rings as a function of radius, and these may be reduced to manageable approximations if the prop is lightly loaded (i.e. close to unit efficiency, unlike a Wake prop). These manipulations do not tell you how to design the prop to achieve the potential efficiencies.

Blade element theory

An alternative approach is required to actually design a propeller or to predict the performance of an existing piece of hardware. This method is based on considering the aerodynamic forces on radial elements of the prop and summing these to give the performance of the total prop. This detail of analysis requires knowledge of how the elements interact - so that the strip lift and drag characteristics have to be modified to account for the apparent aspect ratio. This is problematic on a propeller and it is preferable to consider the overall down-wash and wake interactions:

Vortex theory

The vortex theory is based on the concept that trailing vortices spring from the rotating blades and pass into the slipstream as vortex sheets. The interference velocity at the blades is the velocity induced by this vortex system and the aerodynamic reaction on any blade element is derived from these velocities in con-

junction with two-dimensional aerofoil characteristics.

Wake calculations of this form are very complex and a simplifying assumption is made that the propeller has a large number of blades. This implies that the velocity has a uniform value around any annulus of the propeller disc and the vortex theory then becomes identical to the blade element theory, including the interference velocities determined by the general momentum theory.

With axial and rotational interference factors a and a' as above, the velocities including interference are as shown in figure A2 for a blade element with resultant flow velocity W .

The lift and drag forces generated by unit span of this section of blade are $1/2\rho c W^2 C_L$ and $1/2\rho c W^2 C_D$ respectively, where c is the blade chord. Resolving into the forward and rotational directions gives the contributions to thrust and torque loading for a radial strip dr as:

$$dT = \frac{1}{2} \rho c W^2 (C_L \cos \phi - C_D \sin \phi) \quad (\text{A9})$$

$$dQ = \frac{1}{2} \rho c W^2 (C_L \sin \phi + C_D \cos \phi) \quad (\text{A10})$$

Expressed in terms of solidity σ instead of blade chord ($\sigma=Bc/(2\pi r)$ where B is the number of blades), substituting:

$$C_y = (C_L \cos \phi - C_D \sin \phi) \quad \text{and} \quad C_x = (C_L \sin \phi + C_D \cos \phi)$$

and writing in terms of the non-dimensional thrust and torque coefficients gives:

$$R \frac{dT_C}{dr} = \sigma \left(\frac{r}{R} \right)^3 (1-a')^2 C_y \sec^2 \phi \quad (\text{A11})$$

$$R \frac{dQ_C}{dr} = \sigma \left(\frac{r}{R} \right)^4 (1-a')^2 C_x \sec^2 \phi \quad (\text{A12})$$

Further analysis leads to expressions for the interference factors in terms of the solidity, flow angle and C_x and C_y coefficients:

$$\frac{a'}{1-a'} = \frac{\sigma C_x}{4 \sin \phi \cos \phi} \quad (\text{A13})$$

$$\frac{a}{1+a} = \frac{\sigma C_y}{4 \sin^2 \phi} \quad (\text{A14})$$

The advance ratio may be derived from the velocity relationships as:

$$\lambda = \frac{r}{R} \frac{1-a'}{1+a} \tan \phi \quad (\text{A15})$$

T_c and Q_c from (A11) and (A12) give the thrust and torque coefficients for the prop, which are required as a function of advance ratio. However, it is not possible to evaluate the functions given in (A11) and (A12) directly for a specific advance ratio. The section characteristics C_L and C_D are assumed to be available as functions of incidence α which is linked to the angle ϕ by $\phi = \theta - \alpha$ where θ is the local blade pitch angle. This simple statement tends to mask a major problem, in that the appropriate data for C_L and C_D as a function of α is very hard to find or derive for model conditions. For our low Reynolds number conditions I have postulated degradations of normal full-size lift and drag performance; in view of the large variations across critical conditions on our blades it would be best to have different properties at different radii and for different forward speeds. I have not implemented such a scheme because of the fundamental lack of data to justify it.

The solution technique used is to take a number of values of α , to calculate ϕ for each (and hence the interference factors a' and a from (A13) and (A14). Then the advance ratio λ corresponding to each α is found from (A15). By interpolation we can then find the α at this radius which corresponds to a particular λ . The contribution to T_c and Q_c for this λ can then be evaluated for this radius from (A11) and (A12). Integrating these T_c and Q_c over the whole radius of the prop gives the thrust and torque coefficients for the prop as a function of advance ratio.

The figures A3, A4, A5 show these non-dimensional coefficients and the efficiency plotted against advance ratio for three sample rubber props. These props have a blade chord taken from Andriukov's prop and are identical except for having true helical geometric blade angles with pitch/diameter ratio of 1, 1.2 and 1.4.

The shape of the torque coefficient curves are interesting, dropping with advance ratio up 0.15, then increasing to a peak at about 0.27 before dropping away at high advance ratio when approaching the windmill state. To try to understand this I looked at the individual blade element contributions to torque. They were all similar and the aerodynamic conditions at the most important element, at 77% radius, are shown in figure A6. The fundamental quantity is the local incidence, shown by the line alpha(degrees), dropping as advance ratio increases. For low advance ratio the element is stalled, with the lift at its maximum value and a considerable drag coefficient. The rapid decay of drag coefficient is responsible for the reduction in torque at low advance ratio, followed by a slight increase under the geometric lift component effect as alpha decreases - a given lift force has a larger compo-

ment contributing to the torque for small alpha than for large alpha. The drop in torque for advance ratio above 0.27 corresponds to the drop in lift as the alpha reduces into the normal operating region.

These plots are still some way removed from practical propeller calculation of the thrust for a given applied torque. The actual values of thrust and torque are obtained from T_c and Q_c via equations (A2) and (A3) together with the definition of λ and the substitution of specific values of speed V and rate of rotation Ω . For the P/D=1.2 prop above, sample thrust and torque curves are shown in figures A7 and A8 against RPM for different forward speeds ranging from stationary through to 12 m/sec.

Looking at the two curves for a flying speed of 8 m/sec, it is seen that the prop needs to be turning at 600 RPM before it generates any thrust. There has to be more than 500 RPM before it actually needs any positive torque - that is at lower RPM it is operating as a windmill, and it is no surprise that it does not develop forward thrust!

Looking at the same data plotted in the other sense, figures A9 and A10 show the variation of thrust and torque with airspeed for various RPM. Less torque is required the faster the aircraft is flying (windmill effect again) and thrust also reduces, possibly after reaching a tuned maximum thrust peak first.

Reference

1 Glauert, H. "Div. L Airplane Propellers". W. F. Durand (ed). (1943). *Aerodynamic Theory*. Volume IV.

List Of Symbols

a	axial interference
a'	rotational interference factor
B	number of blades
c	blade chord at radius r
n	propeller speed, revolutions per second
P	power
Q	torque
Q_c	propeller torque coefficient
R	propeller radius
r	radial position
S_1	cross sectional area of the wake
T	thrust
T_c	propeller thrust coefficient
u	velocity at the propeller disc
u_1	final velocity in the wake
V	airspeed (initial inflow velocity upstream of the propeller)
α	incidence
η	efficiency
θ	blade pitch angle at radius r
λ	advance ratio
σ	solidity
Ω	angular velocity of propeller (rad/sec)

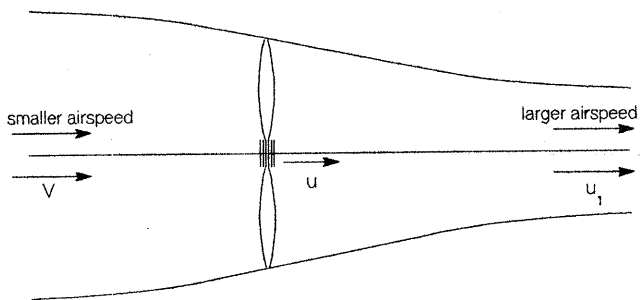


Figure A1. Airflow through a propeller.

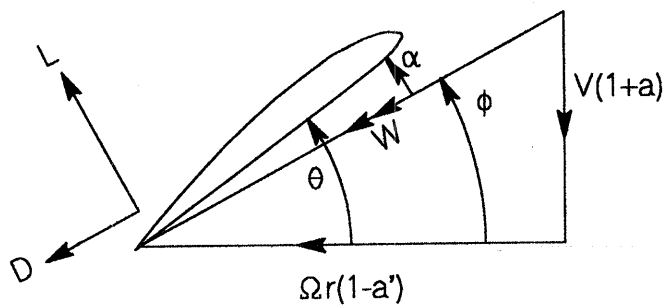


Figure A2. Angles, forces and velocities at a blade element.

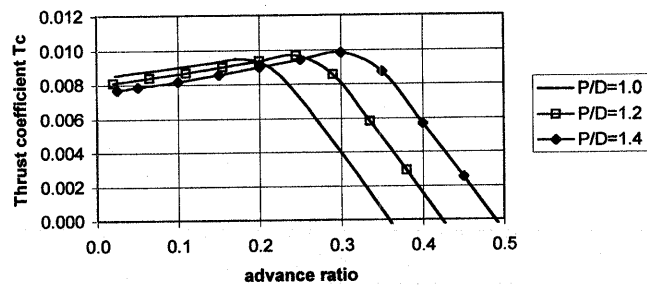


Figure A3. Thrust coefficient for three propellers.

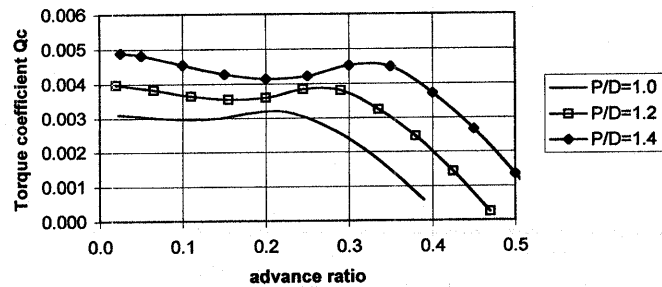


Figure A4. Torque coefficient for three propellers.

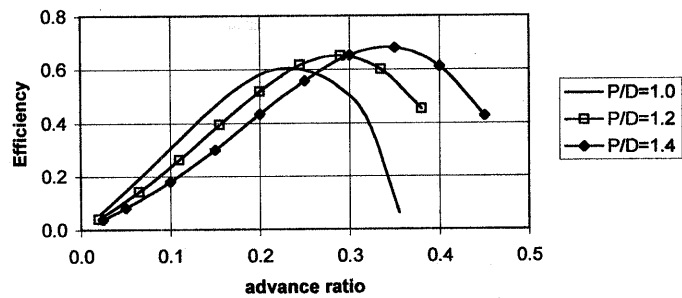


Figure A5. Efficiency of three propellers.

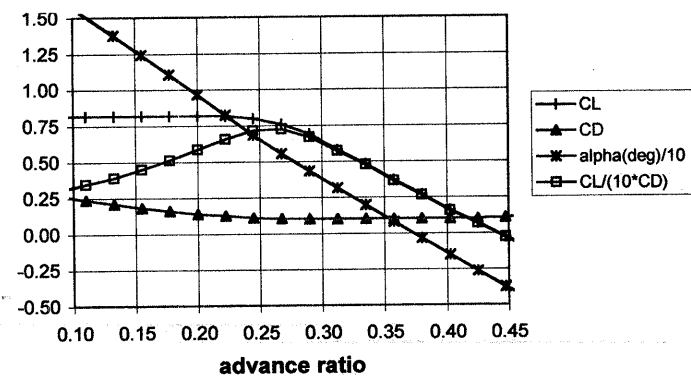


Figure A6. Local aerodynamic quantities at a blade element at 77% radius for the P/D=1.2 propeller.

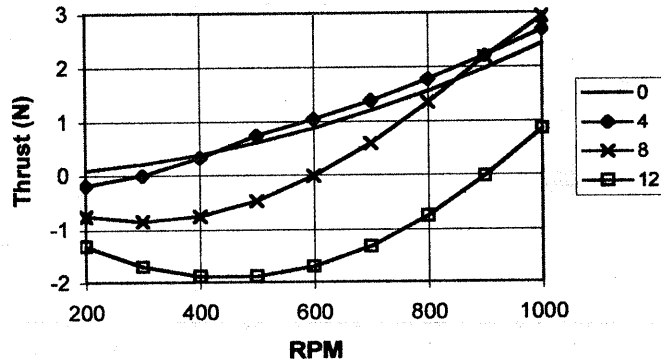


Figure A7. Thrust of the P/D=1.2 propeller for forward speeds 0 to 12 m/sec.

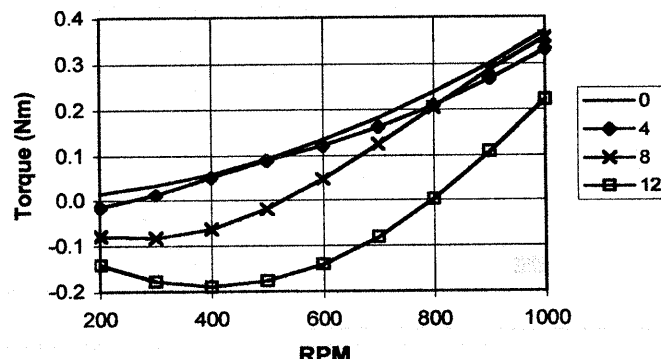


Figure A8. Torque of the P/D=1.2 propeller for forward speeds 0 to 12 m/sec.

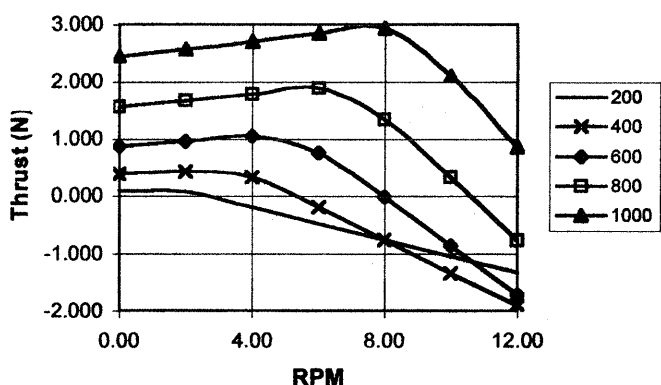


Figure A9. Thrust of the $P/D=1.2$ propeller for RPM from 200 to 1000.

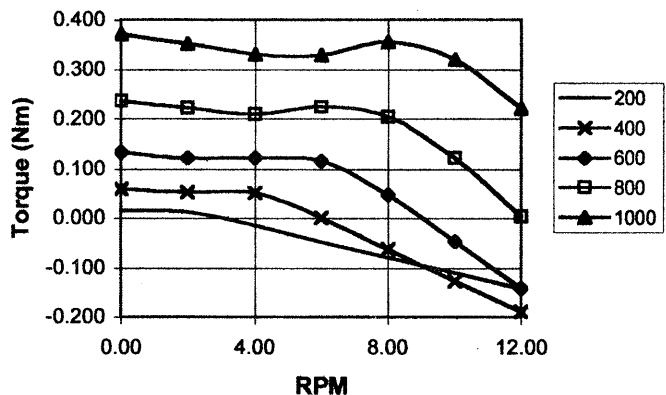
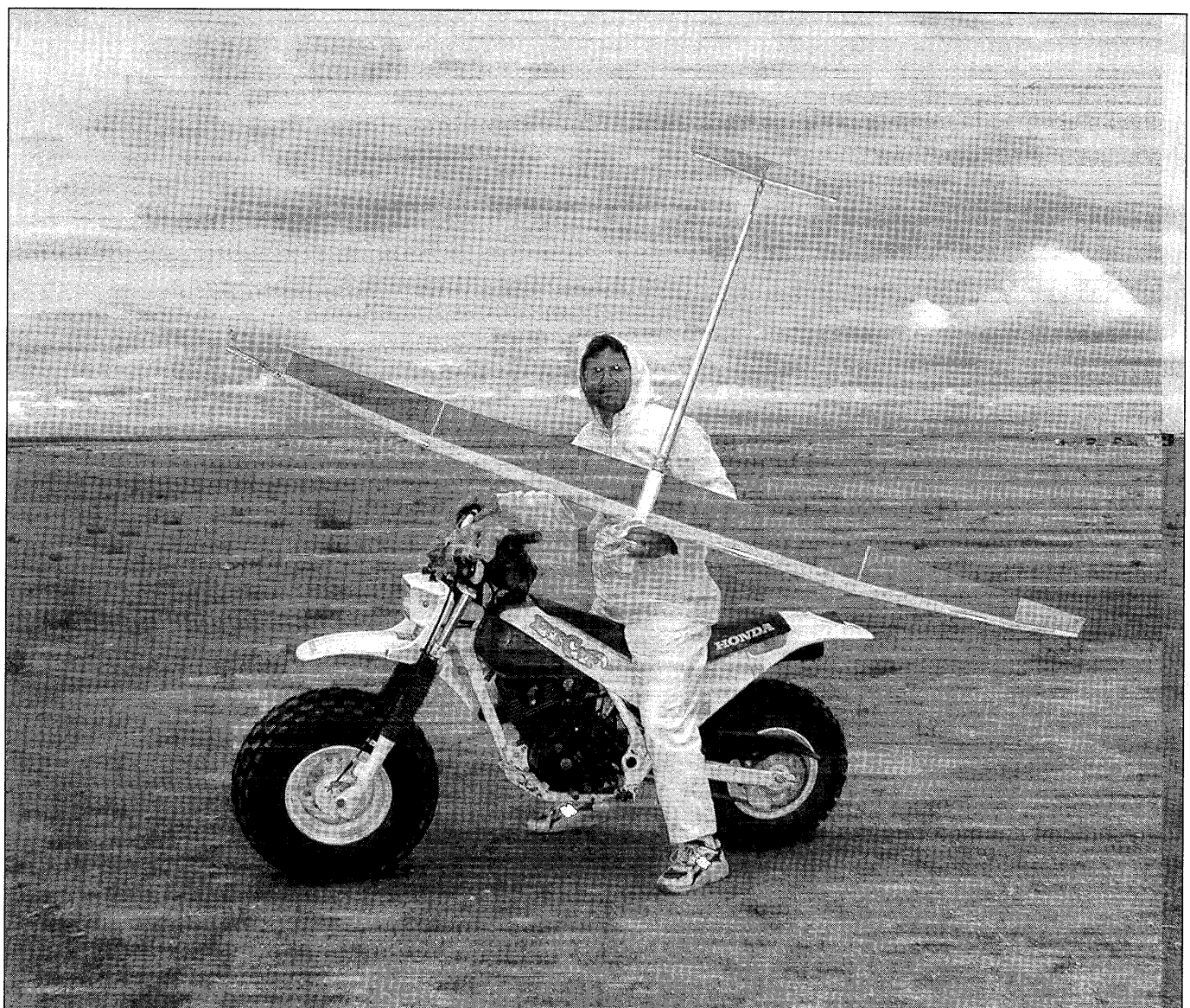


Figure A10. Torque of the $P/D=1.2$ propeller for RPM from 200 to 1000.



Norm Poti